ACS Chemical Neuroscience

Research Article

pubs.acs.org/chemneuro

Kinetic Diversity of Striatal Dopamine: Evidence from a Novel Protocol for Voltammetry

Seth H. Walters, Elaine M. Robbins, and Adrian C. Michael*

Department of Chemistry, University of Pittsburgh, Pittsburgh, Pennsylvania 15260, United States

ABSTRACT: *In vivo* voltammetry reveals substantial diversity of dopamine kinetics in the rat striatum. To substantiate this kinetic diversity, we evaluate the temporal distortion of dopamine measurements arising from the diffusion-limited adsorption of dopamine to voltammetric microelectrodes. We validate two mathematical procedures for correcting adsorptive distortion, both of which substantiate that dopamine's apparent kinetic diversity is not an adsorption artifact.

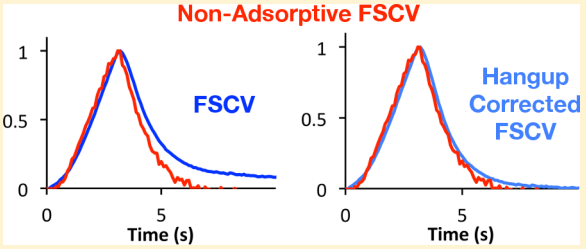

KEYWORDS: *Dopamine, voltammetry, kinetic diversity, modeling, restricted diffusion*

Quantitative kinetic analysis of neurotransmitter release, clearance, and diffusion[1−32] is a valuable contribution to the study of neurotransmission. This report focuses on the kinetic analysis of electrically evoked dopamine (DA) responses recorded by fast-scan cyclic voltammetry (FSCV) in the rat striatum. Previous work shows that such responses can be objectively classified as belonging to several fast and slow kinetic types,[33−39] which reveals the substantial diversity of dopamine kinetics in the dorsal[33−37] and ventral[38,39] striatum.

To substantiate DA's kinetic diversity, it is necessary to validate FSCV's kinetic fidelity. The kinetic fidelity of *in vivo* electrochemical techniques has been questioned rather often.[40−48] Recently,[41] slow-type evoked DA responses were attributed to the temporal distortion of FSCV recordings[40−43] by the diffusion-limited adsorption of DA to the electrodes. Mathematical removal of the distortion eradicated the slow-type response features.[41] Accordingly, the slow-type responses and DA's kinetic diversity must be viewed as FSCV artifacts.

Herein we evaluate adsorptive distortion in a direct manner by recording DA with an FSCV protocol that eliminates DA adsorption. Our results confirm that the slow-type evoked response features are not a product of DA adsorption. We validate two mathematical procedures that correct adsorptive distortion. We emphasize that DA adsorption is highly beneficial in FSCV:[46,49,50] it increases the signal-to-noise ratio, sensitivity, and selectivity of FSCV with only minor and easily managed effects on the temporal response. This work substantiates that DA's kinetic diversity with the striatum is not a FSCV artifact.

RESULTS AND DISCUSSION

Two FSCV Protocols: Waveforms A and B. Waveform A holds the potential at 0.0 V (voltages vs Ag/AgCl) and sweeps first in the positive direction to +1.0 V, then in the negative direction to −0.5 V, and then back to 0.0 V (Figure 1A). DA is not oxidized at 0.0 V, so as usual,[40,42,43,49,51] it adsorbs to the electrode between the FSCV scans. The oxidation of adsorbed DA leads to a large and nearly symmetric voltammetric peak near +0.7 V (Figure 1B): the peak symmetry is indicative of adsorption.[52] Oxidation of DA produces dopamine-*o*-quinone (DoQ), which reduces back to DA near −0.2 V.

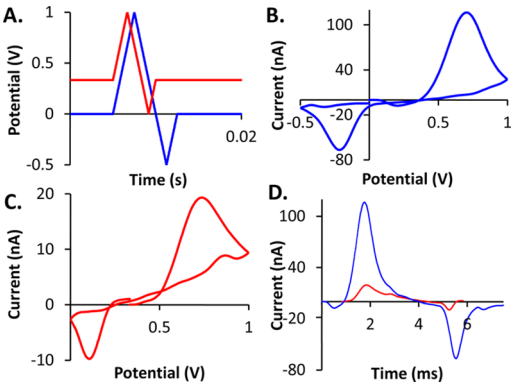

Figure 1. (A) Waveforms A (blue) and B (red), (B) cyclic voltammogram of DA produced by waveform A, (C) cyclic voltammogram of DA produced with the same electrode by waveform B, and (D) the same voltammograms plotted versus time instead of potential.

Waveform B holds the potential at +0.33 V and sweeps to +1.0, 0.0, and +0.33 V (Figure 1A). Oxidation of DA at +0.33 V prevents it from adsorbing to the electrode. For this reason, waveform B produces a smaller and more asymmetrical DA oxidation peak (Figure 1C): the peak asymmetry is indicative of diffusion.[52] Waveform B produces a DoQ reduction peak near +0.2 V during the third segment of the waveform, that is, as the potential is being swept from 0 V back to +0.33 V. Thus, the DoQ reduction peak appears at different potentials when waveforms A and B are used. This is a kinetic effect: when the

Received: January 22, 2016
Accepted: February 17, 2016
Published: February 17, 2016

DOI: 10.1021/acschemneuro.6b00020
ACS Chem. Neurosci. 2016, 7, 662−667

voltammograms are plotted against time, the DoQ peaks line up as expected (Figure 1D).

FSCV postcalibration in a flow cell with waveforms A and B produces different response profiles (Figure 2A). Due to DA

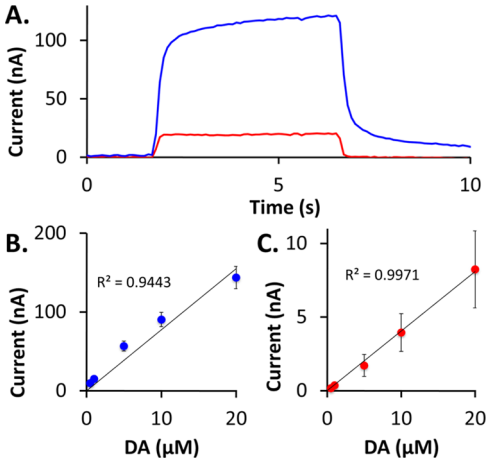

Figure 2. (A) Temporal profiles obtained during electrode postcalibration (DA = 20 μM) with waveforms A (blue) and B (red), (B) DA calibration curve produced by waveform A, and (C) DA calibration curve produced by waveform B. In panels B and C, each data point is the average from postcalibration of n = 6 different electrodes. Error bars in panels B and C are SEM.

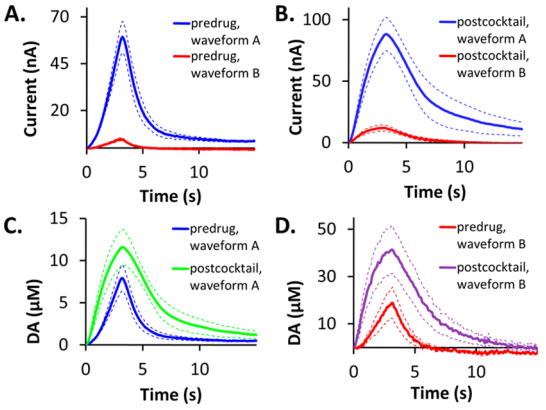

Figure 3. (A) Predrug responses (current) obtained with waveforms A (blue) and B (red), (B) postdrug responses (current) obtained with waveforms A (blue) and B (red), (C) pre- and postdrug responses (concentration) obtained with waveform A, and (D) pre- and postdrug responses (concentration) obtained with waveform B. The solid lines are the average of n = 6 responses obtained with n = 6 electrodes in n = 6 rats. The dashed lines are the standard errors. The stimulus was delivered for 3 s (beginning at t = 0) at 60 Hz. The drug cocktail contained nomifensine (20 mg/mg) and raclopride (2 mg/kg) and was delivered i.p. As determined by two way ANOVA with repeated measures, the drug cocktail significantly affected the evoked responses (C, D) obtained with both waveforms A (p = 0.003) and B (p = 0.016).

adsorption, waveform A produces a larger response that is delayed in reaching its maximum and in returning to its baseline when the DA bolus arrives and departs. Due to the absence of DA adsorption, waveform B produces a smaller response that rapidly rises and falls. Thus, eliminating DA adsorption increases FSCV's temporal response but at the expense of ~15-fold loss in sensitivity. Because adsorption follows an isotherm, such as the Langmuir isotherm, waveform A produces a nonlinear calibration curve with a correlation coefficient less than 1 (Figure 2B). The nonlinearity is slight, however, and has no noticeable effect on the calibration of *in vivo* responses: we routinely use the linear regression (Figure 2B, black line) for calibration purposes. Waveform B produces a linear calibration curve with a correlation coefficient close to 1 (Figure 2C), as expected in the absence of adsorption.

Recording of Evoked DA Responses with Waveforms A and B. Waveforms A and B produce different FSCV responses during recordings of evoked DA release in the striatum (Figure 3A,B). Waveform B produces ~15-fold less voltammetric current, consistent with its lower sensitivity for DA (Figure 2). Postcalibration of the responses obtained with waveforms A (Figure 3C) and B (Figure 3D) leads to three notable differences. First, there is a systematic difference between the DA amplitudes obtained with waveforms A and B. Second, waveform A produces responses that hang up,[31] that is, that do not return to baseline after the stimulus. Third, waveform B produces a lower signal-to-noise ratio and more baseline drift.

There are two likely contributing factors to the different DA amplitudes obtained with waveforms A and B. One is waveform B's low signal-to-noise ratio. Standard approaches in analytical chemistry define the detection limit as the signal that is 3× the noise and the limit of quantitation as 10× the noise.[53] The signal amplitudes produced by waveform B do not exceed 10× the noise, so DA quantitation by this waveform is unreliable. A second contributing factor could be the presence in brain tissue of high concentrations of ascorbic acid (AA), which is well-known to reduce DoQ to DA.[43,47,54] This reaction affects the DA concentration in the vicinity of the electrode while it is at the hold potential (+0.33 V) of waveform B. Thus, the elimination of adsorption also decreases FSCV's selectivity for DA. We did not investigate this matter further because waveform A provides higher signal-to-noise ratio and measures DA without interference by AA.[43,47,54,55]

The Temporal Profiles of Responses with Waveforms A and B. Figure 4 compares the temporal profiles of calibration and *in vivo* evoked responses produced by waveforms A and B. To facilitate the comparison, three manipulations of the data were performed. First, in the case of waveform B, where necessary, a correction was applied for baseline drift (see in Figure 3D where the red trace drifts below the baseline). Second, in the case of waveform A the responses were corrected for hang-up by the procedure explained in Walters et al.[31] (see Methods). Third, the responses were normalized with respect to their maximum amplitude.

Figure 4 validates the hang-up correction procedure based on eq 1 (see Methods) and substantiates that slow-type response features (Figure 4B) are not a product of adsorptive distortion. After the corrections for baseline drift and hang-up, only the in vitro calibration responses exhibit a noticeable temporal difference (Figure 4A). It must be emphasized, however, that the flow system used for calibration causes very rapid changes in the DA concentration, much faster than those observed during *in vivo* FSCV.

The precocktail responses exhibit slow-type features, including an initial lag in the signal when the stimulus begins and a "concave-upwards" profile of the ascending phase of the response (Figure 4B). The ability of the drug cocktail to eliminate the slow response features (Figure 4C), even with the same electrodes in the same recording locations, confirms that

DOI: 10.1021/acschemneuro.6b00020
ACS Chem. Neurosci. 2016, 7, 662−667

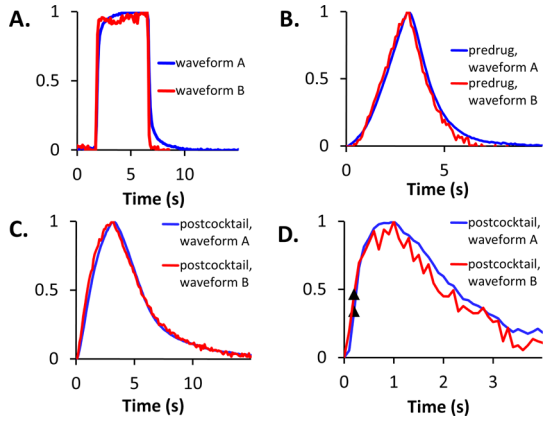

Figure 4. Comparisons of the temporal profiles of responses obtained with waveforms A (blue) and B (red). Responses obtained with waveform A were corrected for hang-up. Responses obtained with waveform B were corrected, as needed, for baseline drift. All responses are normalized to their maximum amplitude. (A) Calibration (representative example from one electrode). (B) Predrug 3-s stimulus responses. (C) Postdrug 3-s stimulus responses. The raw data for panels B and C are shown in Figure 3. (D) Postdrug 200 ms stimulus responses (average of $n = 6$ responses obtained with the same electrodes and animals as B and C). Triangles denote the end of the stimulus. SEM omitted from panels B, C, and D for clarity.

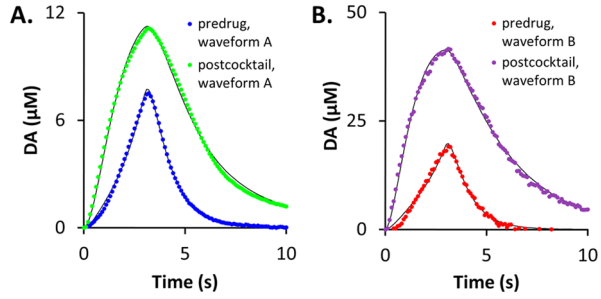

	R_p (zmols)	k_U (s^{-1})	k_T (s^{-1})	k_R (s^{-1})
Waveform A predrug	1.0 ± 0.1*	2.0 ± 0.6**	1.6 ± 0.3***	-0.6 ± 0.1†
Waveform A postcocktail	5.6 ± 1.1*	0.7 ± 0.1**	0.7 ± 0.1***	0.4 ± 0.2†
Waveform B predrug	7.9 ± 5.0‡	7.9 ± 5.6	2.1 ± 0.4	-0.7 ± 0.1§
Waveform B postcocktail	42.0 ± 13.5‡	2.0 ± 1.4	1.1 ± 0.5	0.7 ± 0.3§

Figure 5. Best fits of the restricted diffusion model (black lines) to pre- and postdrug evoked responses (3 s, 60 Hz) obtained with (A) waveform A (corrected for hang-up) and (B) waveform B (corrected for baseline drift). The table reports the corresponding parameter values. With waveform A, all parameter values were significantly different after the administration of the drug cocktail: *R_p ($p = 0.0022$), **k_R ($p = 0.00028$), ***k_U ($p = 0.046$), and †k_T ($p = 0.0083$). With waveform B, only ‡R_p ($p = 0.039$) and §k_R ($p = 0.00049$) were significantly different after the administration of the drug cocktail, while k_U ($p = 0.34$) and k_T ($p = 0.12$) were not significantly different.

the slow features are not due to inherent temporal limitations of the recording technique.

Figure 4D reports postcocktail responses to a 200 ms (12-pulse) stimulus. These responses exhibit the feature called overshoot,[32,35,36,39] where the evoked response continues to rise after the end of the stimulus. The results show that the temporal features of the overshoot are likewise unaffected by DA adsorption.

Figure 4 confirms that adsorptive distortion does not explain the difference between the DA concentrations obtained with waveforms A and B (Figures 3C,D). Theoretically, adsorption would decrease the apparent DA concentration by dampening the FSCV response, but no such dampening is evident in Figure 4.

Kinetic Analysis with the Restricted Diffusion Model. Figure 4 substantiates that the slow-type response features of lag and overshoot are not produced by adsorptive distortion. This is point is important because explaining lag and overshoot has been a challenge. Recently, we introduced a restricted diffusion model[31,32] (see Methods) that explains lag and overshoot. The restricted diffusion model provides excellent fits (Pearson's $r^2 > 0.995$ for each case where the average of the modeled fits is compared with the average of the data) to the pre- and postcocktail responses obtained with waveforms A (hang-up corrected) and B (Figure 5).

The parameters obtained with the model (lower part of Figure 5) show generally good agreement between waveforms A and B. However, waveform B produced parameters with larger standard deviations that diminish their statistical significance. But, some general observations are useful. First, waveforms A and B produced different values of R_p because of the concentration differences explained above. Even so, the magnitude of the change in R_p induced by the cocktail is similar, ~7-fold in each case. Second, there are no significant differences between the values of k_U, k_T, or k_R obtained with waveforms A and B (statistical details in the figure legend). This is because these parameters are first order rate constants determined mainly by the temporal profile, rather than amplitude, of the responses. Both waveforms show that the cocktail, which includes nomifensine, decreases the rate constant for DA uptake, k_U. The decrease in k_U reported by waveform A was significant.

We also modeled postcocktail 200 ms stimulus responses (Figure 6; as reported before,[33,36] slow sites do not respond to a predrug 200 ms stimulus). Again, waveform B produced a larger concentration estimate and a lower signal-to-noise ratio. As we have explained before,[32] these brief stimulus responses can be fit with a simplified three-parameter version of the restricted diffusion model that omits the plasticity factor, k_R. Waveform B produces a larger value of R_p to account for the larger apparent concentration, whereas the two waveforms produce similar values of the rate constants, k_U and k_T (statistical details in the figure legend).

Hang-up Correction via Deconvolution. The key to successful deconvolution is knowledge of the transfer function. In principle, it should be possible to calculate a transfer function for the purpose of hang-up correction from the responses measured with waveforms A and B. In practice, such a calculation was not feasible due to noise contributions. As an alternative approach, we calculated transfer functions from the models of best fit to the responses. To validate this approach, we calculated transfer functions from the best fits to the pre- and postcocktail 3-s responses (Figure 3), used the transfer functions for deconvolution of the responses recorded with waveform A, and compared the outcome with the responses recorded with waveform B. The excellent agreement (Figure 7a) validates deconvolution as a procedure for hang-up correction but emphasizes that the right transfer function must be used.

Next, we examined deconvolution of the *in vivo* responses using the transfer function obtained from best fits to the *in vitro* calibration responses. In this case, deconvolution did not produce good amplitude agreement with the *in vivo* response, but this is again due to the concentrations differences obtained

DOI: 10.1021/acschemneuro.6b00020
ACS Chem. Neurosci. 2016, 7, 662−667

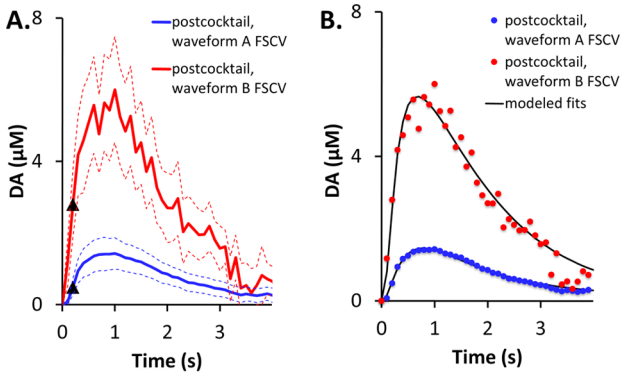

	R_p (zmols)	k_U (s^{-1})	k_T (s^{-1})
Waveform A	4.6 ± 1.2*	1.1 ± 0.3	1.6 ± 0.3
Waveform B	18.2 ± 3.4*	1.6 ± 0.4	2.6 ± 0.8

Figure 6. (A) Postdrug responses to a 200 ms stimulus obtained with waveforms A (blue) and B (red). Solid line is the average of $n = 6$ responses each obtained with a different electrode in a different animal. Dashed lines are the SEM. (B) Best fits of the restricted diffusion model (black lines) to the data points from panel A. The table gives the corresponding parameter values. The R_p, k_U, and k_T parameter values as measured with the two waveforms were also tested for significant differences by an independent sample two tailed t test. The k_U ($p = 0.48$) and k_T ($p = 0.28$) parameter values are not significantly different when measured with either waveform, although the $*R_p$ is significantly ($p = 0.0034$) different when measured with the different waveforms. As determined by two way ANOVA with repeated measures, the waveform used significantly affected the evoked response ($p = 0.017$).

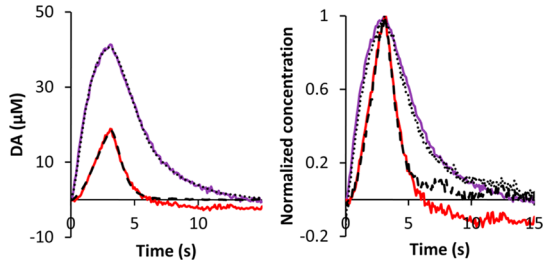

Figure 7. (left) Deconvolutions (black lines) obtained from the waveform A modeled fits and transfer functions derived from the waveform A and waveform B modeled fits to *in vivo* data obtained with waveform B. (right) Normalized deconvolutions (black lines) obtained from deconvolution of waveform A measurements with a transfer function derived from flow cell measurements of waveform A and waveform B and normalized waveform B data (blue and red lines).

with waveforms A and B (Figures 3C,D). However, deconvolution produced excellent agreement with the temporal profiles of the normalized responses (Figure 7B).

The key distinction between this work and the recent literature on deconvolution[41,43] is that the transfer function used here was obtained from *in vitro* calibration by FSCV. When the transfer function is obtained in this way, deconvolution preserves the slow-type features of the precocktail responses and does not produce a poststimulus DA dip below "zero". This confirms our previous speculation that the transfer function employed for kinetic calibration[41] overestimated[40] the effect of adsorption on the temporal response of FSCV.

CONCLUSION

This work substantiates that DA's apparent kinetic diversity is not an artifact of adsorptive distortion. The same FSCV electrodes in the same recording locations produce both fast-type (postcocktail) and slow-type (predrug) responses, which would be impossible if the temporal response of FSCV were adsorption limited.

This work validated two procedures for adsorption correction. Validation was achieved by direct comparison with responses measured without DA adsorption. While useful for validation purposes, neither procedure strictly requires *in vivo* measurements with waveform B. However, calibration with waveform B is necessary for the deconvolution procedure. A novel aspect of our approach is the use of best-fit models to eliminate noise from the transfer functions.

Waveforms A and B produced different estimates of *in vivo* DA concentration. This is likely due to the low signal-to-noise ratio (see Figure 6) and selectivity of waveform B during *in vivo* measurements. Although waveform B is useful in some respects, we do not advocate it for routine use as a substitute for waveform A. Waveform A produces higher sensitivity, signal-to-noise ratio, and selectivity over ascorbate.

The main conclusion stemming from this work is that slow-type evoked responses, which are prevalent throughout the dorsal and ventral striatum,[33,35,36,38,39] are not artifacts produced by adsorptive distortion during *in vivo* FSCV recordings.[41] A recent study in which slow-type response features were eradicated by deconvolution[41] relied on transfer functions obtained with a voltammetric protocol called FSCAV.[56] However, because FSCAV and FSCV exhibit different temporal responses transfer functions obtained via FSCAV cannot be used for deconvolution of responses recorded via FSCV. Indeed, the recent study in question did not include validation of the deconvolution procedure, therein called kinetic calibration. Knowledge of the correct transfer function is critical when deconvolution is performed.

METHODS

The methods employed for this study are similar to those used in prior recent work from our laboratory[33,35−38] with the exception of the new FSCV waveform, waveform B.

FSCV. Carbon fiber electrodes (7 μm in diameter and 200 μm in length) were prepared with T650 fibers (Cytec LLC, Piedmont, SC, USA). The electrodes all received a mild electrochemical pretreatment *in vivo*, consisting of 5 min of scanning at 60 Hz waveform application frequency at 400 V/s waveform beginning at 0.1 V, rising to 1.3 V, falling to −0.5 V, and rising again to the 0.1 V resting potential. The electrodes were then allowed to stabilize for 30 min under the application of waveform A prior to any reported measurements. The details of our conventional FSCV waveform, waveform A, and the new waveform that eliminates DA adsorption, waveform B, are given in Figure 1A and are explained in the opening section of Results and Discussion. The voltage sweep rate for both waveforms was 400 V/s, and both waveforms were applied at 10 Hz. The waveform B measurements were repeated up to 3 times at each recording site to partially alleviate the low signal-to-noise ratio by signal averaging; this was especially helpful for reducing noise in the 12 pulse, 60 Hz stimulus recordings. Where multiple recordings were taken, they were averaged together and treated as a single measurement for the purposes of model fitting and statistical analysis. FSCV was performed with a fast-scan potentiostat (EI-400, out of production) and CVTarHeels software (courtesy Prof. Michael Heien, University of Arizona). FSCV calibration was performed in a homemade flow cell using DA (Sigma, St Louis, MO, USA) dissolved in N_2-purged artificial

DOI: 10.1021/acschemneuro.6b00020
ACS Chem. Neurosci. 2016, 7, 662−667

cerebrospinal fluid (142 mM NaCl, 1.2 mM $CaCl_2$, 2.7 mM KCl, 1.0 mM $MgCl_2$, 2.0 mM NaH_2PO_4, pH 7.4).

Subjects and *in Vivo* Procedures. All procedures involving animals were approved by the University of Pittsburgh Animal Care and Use Committee. Rats (male, Sprague−Dawley, 250−450 g, Charles River Inc., Wilmington, MA) were anesthetized with isoflurane (2.5% by volume O_2), placed in a stereotaxic frame (David Kopf, Tujunga, CA), and connected to an isothermal blanket (Harvard Apparatus, Holliston, MA). Carbon fiber electrodes and stimulating electrodes (MS303/a, Plastics One, Roanoke, VA) were implanted in the dorsal striatum and ipsilateral medial forebrain bundle. The stimulus waveform was a biphasic constant current square wave (2 ms pulses, 60 Hz, 250 μA, 200 ms or 3 s in duration) delivered with a stimulus isolation unit (Neurolog 800, Digitimer, Letchworth Garden City, UK). Alternating between waveform A and waveform B, we recorded evoked responses before and after ip administration of a cocktail containing 2 mg/kg raclopride and 20 mg/kg nomifensine.

Hang-up Correction. The hang-up correction was explained in detail[31] by Walters et al., 2015. Briefly, the algorithm assumes that DA undergoes first order adsorption and desorption at the surface of the FSCV electrode according to the following rate expression:

$$\frac{dH}{dt} = k_{on}C - k_{off}\Gamma_{DA} \quad (1)$$

which is used to construct a hang-up signal component, $H(t)$, by curve fitting to the hang-up segment of the measured response. The correction is performed by subtracting the calculated signal component from the measured response.

In performing the hang-up correction, it is important to avoid distorting DA's apparent kinetics. This could occur, for example, by curve-fitting $H(t)$ to the measured response before the time where the measured response is caused solely by hang-up. To avoid this outcome, we fit $H(t)$ to later and later segments of the reponse until $H(t)$ stops changing.

The DA Kinetic Model. The DA kinetic model has been explained and used in prior recent reports[31,32,37] from our laboratory. It is intended to provide a generic description of restricted diffusion in the brain extracellular space. To do so, it treats the extracellular space as if it were divided into an inner and outer compartment. The model postulates that DA is released into the inner compartment and undergoes restricted diffusion to the outer compartment where it is detected by the FSCV electrode. Uptake then removes DA from the outer compartment. The model is composed of two equations:

$$\frac{dDA_{ic}}{dt} = R_p f\, e^{-k_R t} - DA_{ic}k_T \quad (2)$$

$$\frac{d[DA]_{oc}}{dt} = \frac{DA_{ic}k_T}{V_{oc}} - [DA]_{oc}k_U \quad (3)$$

for the amount of DA in the inner and outer compartments, DA_{ic} (in moles) and $[DA]_{oc}$ (in concentration), respectively. There are four adjustable parameters; R_P represents the moles of DA released per stimulus pulse, k_R is a first order rate constant that modifies DA release, k_T is a first-order rate constant for transport between the compartments, and k_U is a first-order rate constant for DA uptake. There are two fixed parameters; V_{oc} is the volume of the outer compartment (16 μm^3, see Walters et al.),[32] and f is the stimulus frequency.

Deconvolution. Deconvolution procedures were carried out in MatLab (version 2015b). Calculation of transfer functions involves inverse Fourier transformation of the input and output functions, division in the frequency domain, and Fourier transformation of the result. To avoid the effects of noise, the input and output functions were obtained from models of best fit to the responses recorded with waveforms A and B.

Statistics. Statistical analysis was performed in Microsoft Excel (t test) and SPSS (ANOVA). All t tests performed were two-tailed, independent sample t tests with an assumption of equal variance. For the two-way ANOVA with repeated measures tests performed for Figure 3, the first 99 data points of the stimuli were tested (9.9 s of comparison). For the two way ANOVA with repeated measures done for Figure 6, the first 40 data points of the stimuli were tested (4.0 s of comparison).

AUTHOR INFORMATION

Notes

The authors declare no competing financial interest.

ACKNOWLEDGMENTS

This work was supported by the NIH (Grant NS086107).

REFERENCES

(1) Wightman, R. M., Amatore, C., Engstrom, R. C., Hale, P. D., Kristensen, E. W., Kuhr, W. G., and May, L. J. (1988) Real-time characterization of dopamine overflow and uptake in the rat striatum. *Neuroscience 25*, 513−523.

(2) Wu, Q., Reith, M. E., Wightman, R. M., Kawagoe, K. T., and Garris, P. A. (2001) Determination of release and uptake parameters from electrically evoked dopamine dynamics measured by real-time voltammetry. *J. Neurosci. Methods 112*, 119−133.

(3) Harun, R., Grassi, C. M., Munoz, M. J., Torres, G. E., and Wagner, A. K. (2015) Neurobiological model of stimulated dopamine neurotransmission to interpret fast-scan cyclic voltammetry data. *Brain Res. 1599*, 67−84.

(4) Harun, R., Hare, K. M., Brough, M. E., Munoz, M. J., Grassi, C. M., Torres, G. E., Grace, A. A., and Wagner, A. K. (2015) Fast-scan cyclic voltammetry demonstrates that L-DOPA produces dose-dependent regionally selective, bimodal effects on striatal dopamine kinetics in vivo. *J. Neurochem.*, DOI: 10.1111/jnc.13444.

(5) Rooney, K. E., and Wallace, L. J. (2015) Computational modeling of extracellular dopamine kinetics suggests low probability of neurotransmitter release. *Synapse 69*, 515−525.

(6) Xiao, N., Privman, E., and Venton, B. J. (2014) Optogenetic control of serotonin and dopamine release in Drosophila larvae. *ACS Chem. Neurosci. 5*, 666−673.

(7) Morris, E. D., Kim, S. J., Sullivan, J. M., Wang, S., Normandin, M. D., Constantinescu, C. C., and Cosgrove, K. P. (2013) Creating dynamic images of short-lived dopamine fluctuations with lp-ntPET: dopamine movies of cigarette smoking. *J. Visualized Exp.*, DOI: 10.3791/50358.

(8) Normandin, M. D., Schiffer, W. K., and Morris, E. D. (2012) A linear model for estimation of neurotransmitter response profiles from dynamic PET data. *NeuroImage 59*, 2689−2699.

(9) Dreyer, J. K., Herrik, K. F., Berg, R. W., and Hounsgaard, J. D. (2010) Influence of phasic and tonic dopamine release on receptor activation. *J. Neurosci. 30*, 14273−14283.

(10) Best, J. A., Nijhout, H. F., and Reed, M. (2010) Serotonin synthesis, release and reuptake in terminals: a mathematical model. *Theor. Biol. Med. Modell. 7*, 34.

(11) Nakano, T., Doi, T., Yoshimoto, J., and Doya, K. (2010) A kinetic model of dopamine- and calcium-dependent striatal synaptic plasticity. *PLoS Comput. Biol. 6*, e1000670.

(12) Best, J. A., Nijhout, H. F., and Reed, M. C. (2009) Homeostatic mechanisms in dopamine synthesis and release: a mathematical model. *Theor. Biol. Med. Modell. 6*, 21.

(13) Montague, P. R., McClure, S. M., Baldwin, P. R., Phillips, P. E., Budygin, E. A., Stuber, G. D., Kilpatrick, M. R., and Wightman, R. M. (2004) Dynamic gain control of dopamine delivery in freely moving animals. *J. Neurosci. 24*, 1754−1759.

(14) Venton, B. J., Zhang, H., Garris, P. A., Phillips, P. E. M., Sulzer, D., and Wightman, R. M. (2003) Real-time decoding of dopamine concentration changes in the caudate-putamen during tonic and phasic firing. *J. Neurochem. 87*, 1284−1295.

(15) Cragg, S. J., and Rice, M. E. (2004) DAncing past the DAT at a DA synapse. *Trends Neurosci. 27*, 270−277.

(16) Schönfuß, D., Reum, T., Olshausen, P., Fischer, T., and Morgenstern, R. (2001) Modelling constant potential amperometry

DOI: 10.1021/acschemneuro.6b00020
ACS Chem. Neurosci. 2016, 7, 662−667

for investigations of dopaminergic neurotransmission kinetics in vivo. *J. Neurosci. Methods 112*, 163−172.
(17) Rice, M. E., and Cragg, S. J. (2008) Dopamine spillover after quantal release: Rethinking dopamine transmission in the nigrostriatal pathway. *Brain Res. Rev. 58*, 303−313.
(18) Wallace, L. J., and Connell, L. E. (2008) Mechanisms by which amphetamine redistributes dopamine out of vesicles: a computational study. *Synapse 62*, 370−378.
(19) Morris, E. D., Yoder, K. K., Wang, C., Normandin, M. D., Zheng, Q.-H., Mock, B., Muzic, R. F., and Froehlich, J. C. (2005) ntPET: a new application of PET imaging for characterizing the kinetics of endogenous neurotransmitter release. *Mol. Imaging 4*, 473−489.
(20) Volz, T. J., Hanson, G. R., and Fleckenstein, A. E. (2006) Measurement of kinetically resolved vesicular dopamine uptake and efflux using rotating disk electrode voltammetry. *J. Neurosci. Methods 155*, 109−115.
(21) Earles, C., and Schenk, J. O. (1998) Rotating disk electrode voltammetric measurements of dopamine transporter activity: an analytical evaluation. *Anal. Biochem. 264*, 191−198.
(22) Burnette, W. B., Bailey, M. D., Kukoyi, S., Blakely, R. D., Trowbridge, C. G., and Justice, J. B. J. (1996) Human norepinephrine transporter kinetics using rotating disk electrode voltammetry. *Anal. Chem. 68*, 2932−2938.
(23) Cragg, S. J., Clarke, D. J., and Greenfield, S. A. (2000) Real-time dynamics of dopamine released from neuronal transplants in experimental Parkinson's disease. *Exp. Neurol. 164*, 145−153.
(24) Peters, J. L., and Michael, A. C. (2000) Changes in the kinetics of dopamine release and uptake have differential effects on the spatial distribution of extracellular dopamine concentration in rat striatum. *J. Neurochem. 74*, 1563−1573.
(25) Lu, Y., Peters, J. L., and Michael, A. C. (1998) Direct comparison of the response of voltammetry and microdialysis to electrically evoked release of striatal dopamine. *J. Neurochem. 70*, 584−593.
(26) Bertram, R. (1997) A simple model of transmitter release and facilitation. *Neural Comput. 9*, 515−523.
(27) Wheeler, D. D., Edwards, A. M., Chapman, B. M., and Ondo, J. G. (1993) A model of the sodium dependence of dopamine uptake in rat striatal synaptosomes. *Neurochem. Res. 18*, 927−936.
(28) Kawagoe, K. T., Garris, P. A., Wiedemann, D. J., and Wightman, R. M. (1992) Regulation of transient dopamine concentration gradients in the microenvironment surrounding nerve terminals in the rat striatum. *Neuroscience 51*, 55−64.
(29) May, L. J., Kuhr, W. G., and Wightman, R. M. (1988) Differentiation of dopamine overflow and uptake processes in the extracellular fluid of the rat caudate nucleus with fast-scan in vivo voltammetry. *J. Neurochem. 51*, 1060−1069.
(30) Fischer, J. F., and Cho, A. K. (1979) Chemical release of dopamine from striatal homogenates: evidence for an exchange diffusion model. *J. Pharmacol. Exp. Ther. 208*, 203−209.
(31) Walters, S. H., Robbins, E. M., and Michael, A. C. (2015) Modeling the Kinetic Diversity of Dopamine in the Dorsal Striatum. *ACS Chem. Neurosci. 6*, 1468−1475.
(32) Walters, S. H., Taylor, I. M., Shu, Z., and Michael, A. C. (2014) A Novel Restricted Diffusion Model of Evoked Dopamine. *ACS Chem. Neurosci. 5*, 776−783.
(33) Moquin, K. F., and Michael, A. C. (2009) Tonic autoinhibition contributes to the heterogeneity of evoked dopamine release in the rat striatum. *J. Neurochem. 110*, 1491−1501.
(34) Moquin, K. F., and Michael, A. C. (2011) An inverse correlation between the apparent rate of dopamine clearance and tonic autoinhibition in subdomains of the rat striatum: A possible role of transporter-mediated dopamine efflux. *J. Neurochem. 117*, 133−142.
(35) Mitch Taylor, I., Jaquins-Gerstl, A., Sesack, S. R., and Michael, A. C. (2012) Domain-dependent effects of DAT inhibition in the rat dorsal striatum. *J. Neurochem. 122*, 283−294.
(36) Taylor, I. M., Ilitchev, A. I., and Michael, A. C. (2013) Restricted diffusion of dopamine in the rat dorsal striatum. *ACS Chem. Neurosci. 4*, 870−878.
(37) Taylor, I. M., Nesbitt, K. M., Walters, S. H., Varner, E. L., Shu, Z., Bartlow, K. M., Jaquins-Gerstl, A. S., and Michael, A. C. (2015) Kinetic diversity of dopamine transmission in the dorsal striatum. *J. Neurochem. 133*, 522−531.
(38) Shu, Z., Taylor, I. M., and Michael, A. C. (2013) The dopamine patchwork of the rat nucleus accumbens core. *Eur. J. Neurosci. 38*, 3221−3229.
(39) Shu, Z., Taylor, I. M., Walters, S. H., and Michael, A. C. (2014) Region- and domain-dependent action of nomifensine. *Eur. J. Neurosci. 40*, 2320−2328.
(40) Kile, B. M., Walsh, P. L., McElligott, Z. A., Bucher, E. S., Guillot, T. S., Salahpour, A., Caron, M. G., and Wightman, R. M. (2012) Optimizing the temporal resolution of fast-scan cyclic voltammetry. *ACS Chem. Neurosci. 3*, 285−292.
(41) Atcherley, C. W., Laude, N. D., Monroe, E. B., Wood, K. M., Hashemi, P., and Heien, M. L. (2015) Improved Calibration of Voltammetric Sensors for Studying Pharmacological Effects on Dopamine Transporter Kinetics in Vivo. *ACS Chem. Neurosci. 6*, 1509−1516.
(42) Bath, B. D., Michael, D. J., Trafton, B. J., Joseph, J. D., Runnels, P. L., and Wightman, R. M. (2000) Subsecond adsorption and desorption of dopamine at carbon-fiber microelectrodes. *Anal. Chem. 72*, 5994−6002.
(43) Venton, B. J., Troyer, K. P., and Wightman, R. M. (2002) Response times of carbon fiber microelectrodes to dynamic changes in catecholamine concentration. *Anal. Chem. 74*, 539−546.
(44) Kume-Kick, J., and Rice, M. E. (1998) Dependence of dopamine calibration factors on media Ca^{2+} and Mg^{2+} at carbon-fiber microelectrodes used with fast-scan cyclic voltammetry. *J. Neurosci. Methods 84*, 55−62.
(45) Kovach, P. M., Ewing, A. G., Wilson, R. L., and Wightman, R. M. (1984) In vitro comparison of the selectivity of electrodes for in vivo electrochemistry. *J. Neurosci. Methods 10*, 215−227.
(46) Gonon, F. G., Fombarlet, C. M., Buda, M. J., and Pujol, J. F. (1981) Electrochemical treatment of pyrolytic carbon fiber electrodes. *Anal. Chem. 53*, 1386−1389.
(47) Stamford, J. A. (1986) Effect of electrocatalytic and nucleophilic reactions on fast voltammetric measurements of dopamine at carbon fiber microelectrodes. *Anal. Chem. 58*, 1033−1036.
(48) Gerhardt, G. A., and Hoffman, A. F. (2001) Effects of recording media composition on the responses of Nafion-coated carbon fiber microelectrodes measured using high-speed chronoamperometry. *J. Neurosci. Methods 109*, 13−21.
(49) Hafizi, S., Kruk, Z. L., and Stamford, J. A. (1990) Fast cyclic voltammetry: Improved sensitivity to dopamine with extended oxidation scan limits. *J. Neurosci. Methods 33*, 41−49.
(50) Heien, M. L., Phillips, P. E., Stuber, G. D., Seipel, A. T., and Wightman, R. M. (2003) Overoxidation of carbon-fiber microelectrodes enhances dopamine adsorption and increases sensitivity. *Analyst 128*, 1413−1419.
(51) Bath, B. D., Martin, H. B., Wightman, R. M., and Anderson, M. R. (2001) Dopamine Adsorption at Surface Modified Carbon-Fiber Electrodes. *Langmuir 17*, 7032−7039.
(52) Bard, A. J., and Faulkner, L. R. (2000) *Electrochemical Methods: Fundamentals and Applications*, Wiley, New York.
(53) Harris, D. C. (2006) *Quantitative Chemical Analysis*, W.H. Freeman, New York.
(54) Kile, B. M., Walsh, P. L., McElligott, Z. A., Bucher, E. S., Guillot, T. S., Salahpour, A., Caron, M. G., and Wightman, R. M. (2012) Optimizing the Temporal Resolution of Fast-Scan Cyclic Voltammetry. *ACS Chem. Neurosci. 3*, 285−292.
(55) Michael, A. C. (1987) Ph.D. Dissertation, Emory University.
(56) Atcherley, C. W., Laude, N. D., Parent, K. L., and Heien, M. L. (2013) Fast-scan controlled-adsorption voltammetry for the quantification of absolute concentrations and adsorption dynamics. *Langmuir 29*, 14885−14892.

DOI: 10.1021/acschemneuro.6b00020
ACS Chem. Neurosci. 2016, 7, 662−667